Neuron, Vol. 29, 185–196, January, 2001, Copyright ©2001 by Cell Press

Disruption of ClC-3, a Chloride Channel Expressed on Synaptic Vesicles, Leads to a Loss of the Hippocampus

Sandra M. Stobrawa,* Tilman Breiderhoff,* Shigeo Takamori,† Dominique Engel,‡ Michaela Schweizer,* Anselm A. Zdebik,* Michael R. Bösl,* Klaus Ruether,§ Holger Jahn,‖ Andreas Draguhn,‡ Reinhard Jahn,† and Thomas J. Jentsch*#

*Zentrum für Molekulare Neurobiologie Hamburg
Universität Hamburg
Martinistrasse 85
D-20246 Hamburg
Germany

†Max-Planck-Institut für Biophysikalische Chemie
Am Faßberg
D-37077 Göttingen
Germany

‡Johannes-Müller-Institut für Physiologie
Humboldt Universität Berlin
Tucholskystrasse 2
D-10117 Berlin
Germany

§Klinik für Augenheilkunde
Universität Hamburg
Martinistrasse 52
D-20246 Hamburg
Germany

‖Klinik für Psychiatrie
Universität Hamburg
Martinistrasse 52
D-20246 Hamburg
Germany

Summary

Several plasma membrane chloride channels are well characterized, but much less is known about the molecular identity and function of intracellular Cl^- channels. ClC-3 is thought to mediate swelling-activated plasma membrane currents, but we now show that this broadly expressed chloride channel is present in endosomal compartments and synaptic vesicles of neurons. While swelling-activated currents are unchanged in mice with disrupted ClC-3, acidification of synaptic vesicles is impaired and there is severe postnatal degeneration of the retina and the hippocampus. Electrophysiological analysis of juvenile hippocampal slices revealed no major functional abnormalities despite slightly increased amplitudes of miniature excitatory postsynaptic currents. Mice almost lacking the hippocampus survive and show several behavioral abnormalities but are still able to acquire motor skills.

Introduction

Chloride channels regulate electrical excitability, the ionic composition of intra- and extracellular compartments, and cell volume. There is solid molecular, biophysical, and physiological information on several plasma membrane Cl^- channels that are involved in synaptic inhibition, transepithelial transport, or muscular excitability. Although intracellular Cl^- channels are thought to play important roles in the secretory and endocytotic pathways and other intracellular organelles, little is known about their properties and molecular identities. Recent evidence indicates that some CLC Cl^- channels normally reside in intracellular membranes (Gaxiola et al., 1998; Günther et al., 1998; Schwappach et al., 1998). CLC channels comprise a large gene family with members in bacteria, yeast, plants, and animals (Jentsch et al., 1999). There are nine CLC genes in mammals that belong to three different branches. The first subfamily encodes plasma membrane Cl^- channels. Their importance is illuminated by diseases resulting from mutations in their genes: loss of function of the muscle Cl^- channel ClC-1 causes myotonia (Steinmeyer et al., 1991), and mutations in two different kidney isoforms impair salt transport across the renal tubule (Simon et al., 1997; Matsumura et al., 1999).

The function of the remaining two CLC subfamilies is less clear. One branch comprises ClC-6 and ClC-7. These channels are broadly expressed, do not yield plasma membrane currents, and probably reside in intracellular organelles (Jentsch et al., 1999). Another branch of the gene family comprises ClC-3, ClC-4, and ClC-5. These proteins are 80% identical and show different tissue distributions. Both ClC-3 and ClC-4 are expressed in brain and many other tissues (Kawasaki et al., 1994; Jentsch et al., 1999), whereas ClC-5 is mainly found in the kidney. The mutational inactivation of ClC-5 in Dent's disease leads to proteinuria (Lloyd et al., 1996), suggesting that it is crucial for the endocytotic removal of proteins from the urine. ClC-5 colocalizes with the H^+-ATPase in endosomes (Günther et al., 1998), and its disruption in mice causes a broad defect in renal endocytosis (Piwon et al., 2000). It probably provides an electrical shunt that is needed for the efficient proton pumping of the electrogenic H^+-ATPase. This concept is supported by the finding that disruption of either the single yeast CLC gene or of a subunit of the V-type H^+-ATPase results in a common phenotype (Greene et al., 1993).

There are conflicting data concerning the function of ClC-3. Some groups reported plasma membrane currents upon expression in *Xenopus* oocytes (Kawasaki et al., 1994) or in transfected 3T3 or CHO cells (Kawasaki et al., 1995; Duan et al., 1997; Shimada et al., 2000). However, there were many differences in their biophysical properties. Furthermore, Kawasaki et al. (1995) described an inhibition of ClC-3 by intracellular calcium, whereas Duan et al. (1997) proposed that ClC-3 underlies the important $I_{Cl,swell}$ current. We have been unable to reproduce these results, and currents from the highly related ClC-4 and ClC-5 channels differ drastically in their properties (Friedrich et al., 1999) from those reported for ClC-3 by Kawasaki et al. (1995) or Duan and coworkers.

To whom correspondence should be addressed (e-mail: jentsch@uke.uni-hamburg.de).

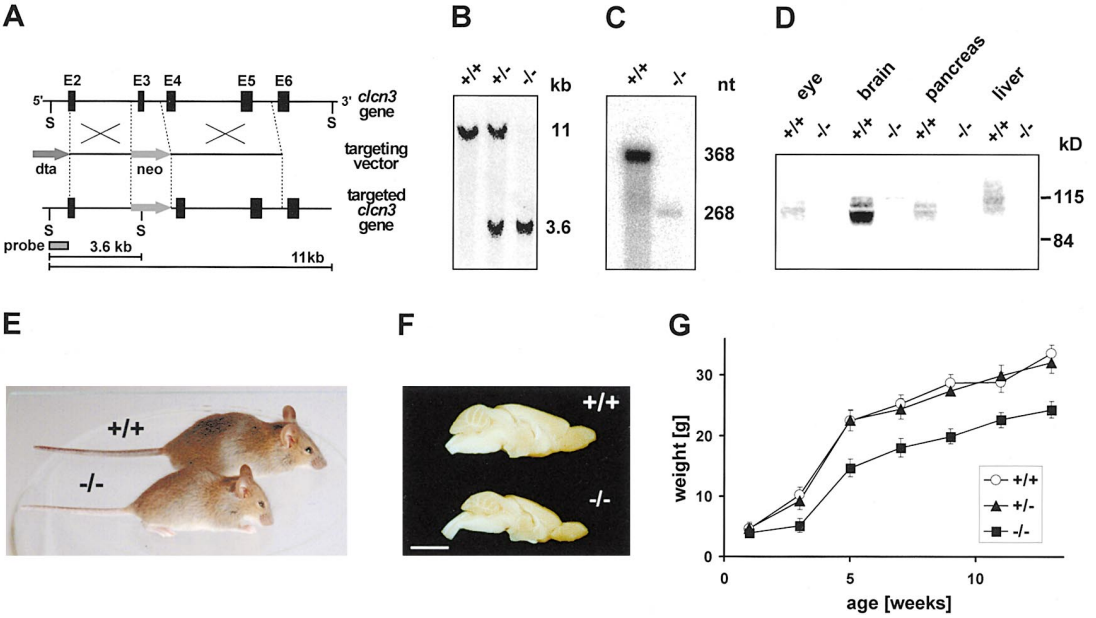

Figure 1. Generation of Mice with a Null Mutation in the *Clcn3* Gene

(A) Targeting of the *Clcn3* gene. The top shows part of the genomic *Clcn3* sequence containing exons 2–6 (black bars). In the targeting vector shown below, 1.1 kb of genomic sequence is replaced by a neomycin (neo) cassette. A diphteria toxin A (dta) cassette was fused to the 5′ end of exon 2 to select against random integration. The disrupted gene is shown below.

(B) Southern analysis of genomic DNA from $Clcn3^{+/+}$, $Clcn3^{+/-}$, and $Clcn3^{-/-}$ mice. DNA was digested with StuI and probed with the probe shown in (A). As the neomycin cassette introduces a novel StuI site (S), the 3.6 kb fragment indicates the null allele.

(C) RNase protection assay using brain RNA from WT and KO mice. The cRNA probe covers 369 nt of the WT *Clcn3* exons 3–5. Deletion of exon 3 yields a 100 bp smaller fragment in the KO.

(D) Western analysis of membrane proteins using the ClC-3 antibody 3A4 reveals that ClC-3 is absent in KO mice.

(E) A 6-week-old $Clcn3^{-/-}$ mouse with a WT littermate. The KO mouse is smaller and arches its back.

(F) Brains dissected from 7-month-old WT (top) and KO mice (bottom). Scale bar: 0.5 cm.

(G) Averaged weights of WT, $Clcn3^{+/-}$, and $Clcn3^{-/-}$ mice ($n \geq 7$ of each genotype) during the first 15 weeks after birth.

To elucidate the cellular and physiological roles of ClC-3, we disrupted the *Clcn3* gene in mice. $Clcn3^{-/-}$ (knockout, KO) mice were viable but smaller than wild-type (WT) littermates. They showed a selective degeneration of the hippocampus that started around postnatal day 12 and led to its nearly complete loss after about 8 weeks. Nonetheless, $Clcn3^{-/-}$ mice survived for more than a year and were able to acquire motor skills. In addition, they completely lost their photoreceptors. KO mice had normal swelling-activated Cl^- currents, in contrast to the proposed function of ClC-3 (Duan et al., 1997). Cell fractionation and immunocytochemistry of transfected cells revealed that ClC-3 is an intracellular channel that is also present on synaptic vesicles. We assumed that it contributes to vesicular acidification by providing an electrical shunt for the efficient proton pumping by the H^+-ATPase. Indeed, synaptic vesicles from KO mice were acidified at slower rates. Electrophysiological analysis of hippocampal slices obtained at the beginning of degeneration did not reveal major defects at the network level, indicating that the functional loss preceding hippocampal degeneration is subtle. However, miniature excitatory postsynaptic currents (mEPSCs) in CA1 pyramidal cells were slightly enhanced in amplitude while inhibitory GABAergic mIPSCs were unchanged, suggesting enhanced vesicular glutamate filling in ClC-3-deficient mice.

Results

Disruption of the *Clcn3* Gene

The *Clcn3* gene was disrupted in embryonic stem cells by replacing a segment of genomic sequence, including exon 3 by a selectable marker (Figure 1A). This deleted a sequence coding for the first transmembrane domain and is predicted to lead to a truncation of the protein. Homozygous $Clcn3^{-/-}$ mice were obtained from heterozygous $Clcn3^{+/-}$ animals at approximately Mendelian ratio. RNase protection assays using brain RNA from WT and KO mice showed a complete absence of normal ClC-3 mRNA in $Clcn3^{-/-}$ mice (Figure 1C). Immunoblotting membrane proteins using a specific antibody directed against the amino terminus of ClC-3 revealed that the protein was absent in KO mice (Figure 1D).

Growth Defect and Degeneration of the Hippocampus

$Clcn3^{-/-}$ mice were smaller than their littermates at all ages except immediately after birth (Figures 1E and 1G). Although they showed overall higher mortality, $Clcn3^{-/-}$ mice survived for more than a year. Dissection of mice older than 3 months showed a drastic reduction of brain size (Figure 1F). Brain sections revealed that the hippocampus was replaced by a large cavity contiguous with the ventricular system (Figures 2A and 2B). The nearly

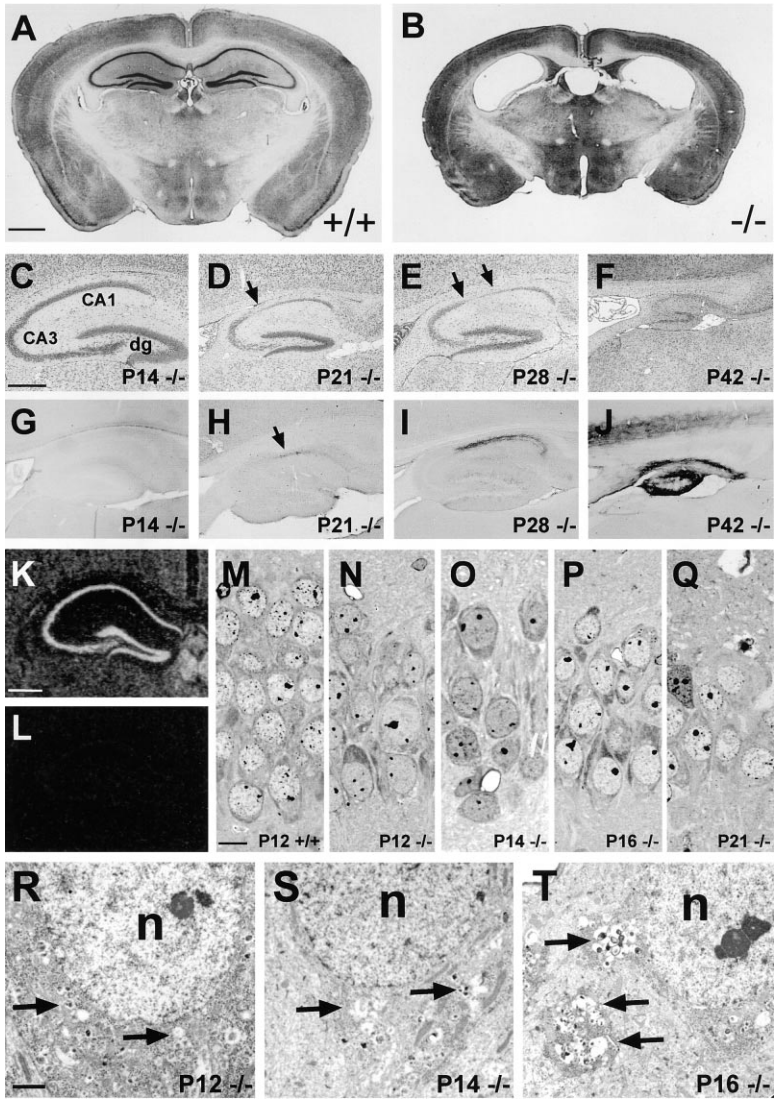

Figure 2. Degeneration of the Hippocampus in *Clcn3*$^{-/-}$ Mice

(A and B) Frontal sections of an adult (7-month-old) WT and KO mouse, respectively (Nissl stain). The hippocampal formation is nearly totally lost in KO.

(C–J) Nissl-stained sagittal sections (C–F) of KO hippocampi from P14 to P42. (G–J) Adjacent sections labeled with GSA for reactive microglia. At P14 (C and G) the hippocampal formation with the dentate gyrus (dg), CA3, and CA1 region is still well preserved. At P21 (D) the number of pyramidal cells has decreased in the CA1 region (arrow), and microglial cells are slightly labeled (arrow in [H]). At P28 the degeneration has spread over the CA1 region (arrows in [E]) and microglial labeling is stronger (I). At P42 (F) pyramidal cells from the CA1 and the CA3 region have disappeared. Only a few granular neurons are found in the dentate gyrus. The remaining hippocampus is labeled strongly for microglia (J).

(K and L) In situ hybridization of adult WT hippocampus using an antisense ClC-3 probe (K) and a sense probe as control (L).

(M–Q) Higher power micrographs from the CA1 region from P12 to P21. Compared to WT (M), the number of pyramidal nuclei is already reduced at P12 in KO mice (N). At P16 (P) almost half of the nuclei are lost and at P21 (Q) parts of the CA1 region are severely damaged.

(R–T) High-power electron micrographs from CA1 region of P12 (R), P14 (S), and P16 (T) KO mice. At P12 first signs of cell degeneration (arrows) can be found around the nucleus (n). At P16 (T) the cytoplasm of many pyramidal cells shows lysis (arrows).

Scale bar: (A) and (B) 1 mm; (C)–(L) 0.5 mm; (M)–(Q) 10 μm; (R)–(T) 1 μm.

complete loss of hippocampal structures in adult KO mice was not due to an early developmental defect but rather was caused by a selective degeneration starting about 2 weeks after birth (Figures 2C–2Q). Activation of microglia (Figures 2G–2J) was detected in the CA1 region around postnatal day 21 (P21), with a progression to CA3 and other regions of the hippocampus at later times (Figures 2I and 2J). Semi-thin sections revealed a loss of pyramidal cells in the CA1 region already at P12 (Figures 2M and 2N). At this time, electron microscopy showed signs of degeneration in the cytoplasm of pyramidal cells (Figure 2R). Cell loss and degeneration of neurons increased over the following weeks (Figures 2O–2Q, 2S, and 2T). Immunohistochemistry using antibodies against several marker proteins (synaptophysin, MAP2) did not reveal gross changes prior to the degeneration. The surprisingly selective cytolysis of the hippocampus fits to the high level of ClC-3 expression in that structure (Figures 2K and 2L) (Kawasaki et al., 1994; Borsani et al., 1995).

The structurally highly related chloride channel ClC-4 is also prominently expressed in the hippocampus (Adler et al., 1997). In situ hybridization (Figure 3A) and RNase protection experiments (Figure 3B) revealed no significant local or global changes of ClC-4 expression in brains of *Clcn3*$^{-/-}$ mice. There was neither a significant change in the mRNA levels of ClC-5 (Figure 3B), another close homolog of ClC-3 that is only weakly expressed in brain (Steinmeyer et al., 1995).

Retinal Degeneration

Clcn3$^{-/-}$ mice were blind as a consequence of a severe retinal degeneration that led to a complete loss of photoreceptors by P28 (Figure 4). The retina appeared normal by light microscopy at P10 (Figure 4A). Electron microscopy revealed a disorganization of photoreceptor outer segments already at P12 (Figure 4B). Between P12 and P28, there was a complete degeneration of photoreceptors, with a loss of outer segments (OS) as well as the nuclei that form the outer nuclear layer (ONL). Immunohistochemistry revealed that ClC-3 is concentrated in the inner and outer plexiform layers (IPL, OPL), the regions of synaptic connections (Figure 4C). In the OPL, where photoreceptors connect to bipolar and horizontal

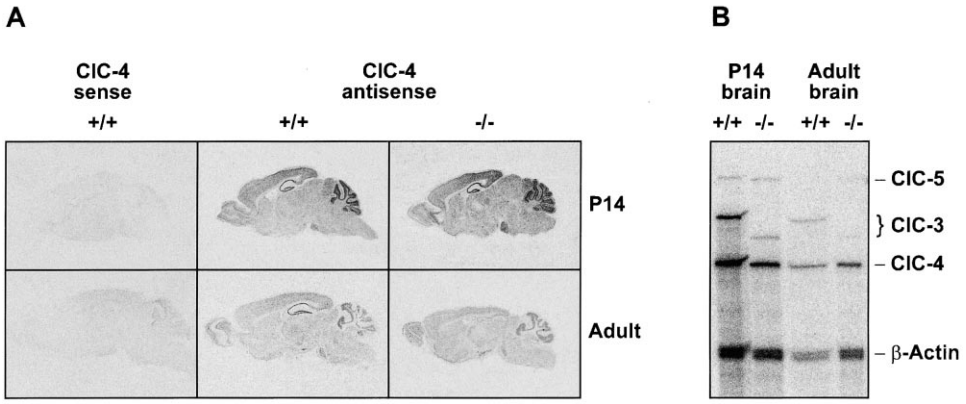

Figure 3. Expression of ClC-4 and ClC-5 in Brains of WT and *Clcn3*$^{-/-}$ Mice

(A) In situ hybridization of P14 and adult brain sections from WT and KO mice. The sense probe (left panel) served as a negative control.
(B) RNase protection assays of the expression of ClC-3, ClC-4, ClC-5, and β-actin (control) in P14 and adult brains of WT and *Clcn3*$^{-/-}$ mice. When normalized to actin, there are no significant changes in the expression levels of ClC-4 or ClC-5 between the genotypes. ClC-5 is only weakly expressed in brain. As the ClC-3 probe includes sequence from the deleted exon, the resulting band is smaller with KO mice.

neurons, expression of ClC-3 overlapped with VGLUT1/BNPI, a protein of glutamatergic synaptic vesicles (Bellocchio et al., 1998).

Electroretinograms

Flash electroretinograms (ERGs) were performed on anesthetized mice as soon as mice opened their eyes (P14 and P15). WT and heterozygous mice showed normal scotopic ERGs characterized by the b wave that mainly reflects the activity of the OPL and INL (inner nuclear layer) and, at higher stimulus intensities, by the a wave mainly representing the response of photoreceptors (Figure 4D). In contrast, *Clcn3*$^{-/-}$ mice either lacked an electrical response (indicating a severe retinal degeneration; registration 1.−/−) or showed a small a wave that was not followed by a detectable b wave (2.−/−). This indicates that the photoreceptors, which can still respond to light, cannot excite the neurons located downstream.

Behavioral Tests

Given the severe neurodegeneration in adult *Clcn3*$^{-/-}$ mice, we performed basic behavioral tests. In open field experiments, WT animals adapted to the new environment by showing less locomotion with time (Figure 5A). In contrast, the locomotion of KO mice increased over the same period. KO mice showed stereotypic running in circles with intermittent short stops over long periods. Increased motor activity was confirmed in actimot tests in which KO mice showed a highly increased basal locomotion compared to WT (3.5 ± 0.8 km versus 1.1 ± 0.6 km per day; mean ± SD, n ≥ 6). This was accompanied by an overall reduced resting time. Under resting conditions, KO mice often arched their back (Figure 1E). In rotarod tests of motor skills, KO mice had initial difficulties and showed tremor when first put onto the rod. However, they improved with time and were able to learn motor skills (Figure 5B).

Swelling-Activated Chloride Currents Are Not Affected by the Loss of ClC-3

ClC-3 is thought to mediate the swelling-activated Cl^- current $I_{Cl,swell}$ that is present in most tissues (Duan et al., 1997). We therefore asked whether swelling-activated Cl^- currents were abolished in *Clcn3*$^{-/-}$ mice and examined two of the many tissues expressing ClC-3 (Figure 1D). Hepatocytes and pancreatic acinar cells from both WT and KO mice displayed typical $I_{Cl,swell}$ currents that were outwardly rectified, inactivated at positive voltages (Figure 6), and displayed the typical $I^- > Cl^-$ conductance. Similar but smaller currents developed slowly also under nominally isotonic conditions, suggesting that cells were slightly swelling upon perfusion with our intracellular solution. Indeed, this current component was abolished by extracellular hypertonicity. There was no significant difference in swelling-activated currents between WT and KO mice (Figure 6B), indicating that ClC-3 does not underlie $I_{Cl,swell}$. An upregulation of the closely related isoforms ClC-4 and ClC-5 in KO mice cannot explain these negative results because currents of ClC-4 and ClC-5 (Friedrich et al., 1999) differ vastly from swelling-activated Cl^- currents in their biophysical properties.

ClC-3 Is a Chloride Channel of Intracellular Vesicles

The finding that ClC-3 does not mediate swelling-activated Cl^- currents, together with the fact that the closely related ClC-5 is present in endosomes (Günther et al., 1998; Piwon et al., 2000), prompted us to investigate the subcellular localization of ClC-3. Liver membrane vesicles were separated on a Percoll gradient and probed for the presence of ClC-3 and marker proteins of intracellular membranes. ClC-3 was present in fractions enriched for the endosomal marker rab4 and showed some overlap with lamp-1, a marker of late endosomes and lysosomes (Figure 7A). In transfected COS-7 cells, ClC-3 was present in numerous small cytoplasmic vesicles (Figure 7D). Its expression did not overlap completely with any of the vesicular marker proteins we used in double-staining experiments. However, almost all vesicles that were positive for ClC-3 also stained for lamp-1, although only a subset of lamp-1 positive vesicles stained for ClC-3.

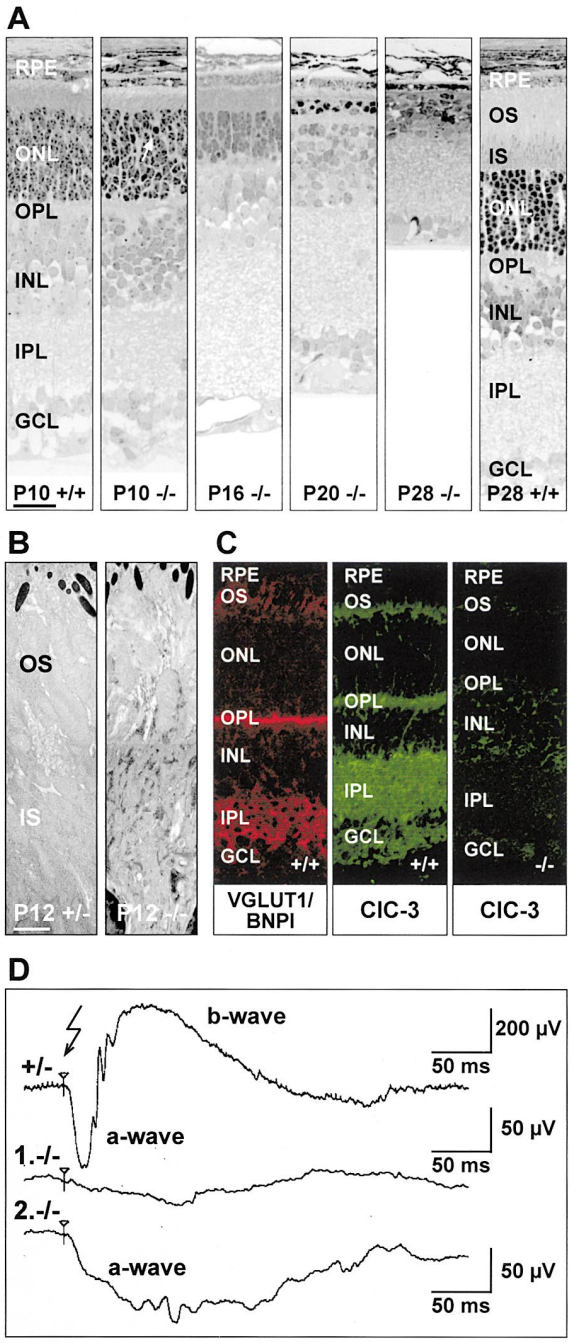

Figure 4. Retinal Degeneration in *Clcn3*$^{-/-}$ Mice

(A) Retinal sections from mice of different ages and genotypes. Several pyknotic nuclei are present in the ONL of the *Clcn3*$^{-/-}$ retina already at P10 (arrow). Photoreceptor degeneration continues until P28 when the ONL is completely missing.

(B) Electron micrographs of the outer and the inner segments (OS, IS) of photoreceptors reveal damage in KO mice already at P12. Their outer and inner segments are highly disorganized.

(C) Immunohistochemistry of retinas (P14–P16) using antibodies against VGLUT1/BNPI and ClC-3 (3A6). VGLUT1/BNPI is found in the OPL and near the ganglion cell layer (GCL), while ClC-3 is more diffusely distributed in the OPL and IPL.

(D) ERG responses of dark adapted retinas from P15 old *Clcn3*$^{+/-}$ and KO mice. Stimulus energy was 3 cds/m^2. *Clcn3*$^{-/-}$ retinas either did not respond (observed in 7 P14 and 4 P15 mice; indicated by 1.−/−) or showed only a small a wave (4 P15 mice; 2.−/−). Scale bar: (A) 50 µm; (B) 2.5 µm.

ClC-3 Is Expressed on Synaptic Vesicles and Is Involved in Their Acidification

Since ClC-3 is highly expressed in brain (Figure 1D), we asked whether it resides on synaptic vesicles. In an established procedure to purify synaptic vesicles from rat brain (Huttner et al., 1983), ClC-3 copurified with the synaptic vesicle protein synaptophysin in the highly enriched "SV" fraction that contains >90% synaptic vesicles (Figure 7B). We further purified synaptic vesicles by immunoisolation on microbeads coated with antibodies (Takamori et al., 2000b) for synaptophysin (a marker of synaptic vesicles in general), VGLUT1/BNPI (a synaptic vesicle glutamate transporter [Bellocchio et al., 2000; Takamori et al., 2000a]), and VGAT (a synaptic vesicle GABA transporter [McIntire et al., 1997]) (Figure 7C). ClC-3 was found in all three subsets of vesicles. We also expressed an epitope-tagged version of ClC-3 in cultured hippocampal neurons from neonatal rats. ClC-3 appeared in structures that are typical for synaptic terminals and colocalized with synaptophysin (Figure 7E). The localization to synapses is also supported by our immunohistochemistry of the retina (Figure 4C).

We compared synaptic vesicle proteins prepared from adult WT and KO mice (Figure 8A). There were no obvious differences in the abundance of the 116 kDa subunit of the H^+-ATPase and several synaptic vesicle proteins (synaptophysin, synaptogyrin, and synaptobrevin). There was also no difference in the GABA transporter VGAT, but a 48% ± 15% (SD, n = 6) reduction in the glutamate transporter VGLUT1/BNPI.

Synaptic vesicles are acidified by a V-type H^+-ATPase that needs a parallel Cl^- conductance for efficient pumping. The resulting electrochemical gradient is important for the uptake of neurotransmitters (Reimer et al., 1998; Gasnier, 2000). The ATP-stimulated acidification of purified synaptic vesicles from either WT or KO mice depended on the presence of Cl^-, but synaptic vesicles from KO mice acidified at lower rates (Figure 8B). We next determined the fraction of vesicular uptake of glutamate and dopamine that was driven by the proton gradient (Figures 8C and 8D). There was no difference in the uptake of dopamine, but glutamate uptake was significantly reduced in KO. Glutamate uptake is known to be driven by the vesicular membrane potential that is determined by the chloride concentration (Maycox et al., 1988). Therefore, we tested glutamate uptake activity at several different chloride concentrations. The relative chloride dependence of glutamate uptake was unchanged in vesicles from KO mice, suggesting that the reduction is due to a selective loss of glutamatergic vesicles (Figure 8C). This correlated with the reduction of the glutamate transporter VGLUT1/BNPI in synaptic vesicles from *Clcn3*$^{-/-}$ mice (Figure 8A).

Electrophysiology of Acute Hippocampal Slice Preparations

To detect possible functional deficits in synaptic transmission, we prepared hippocampal slices from WT and KO mice between P13 and P15. At this age, ultrastructural alterations are already present in CA1 pyramidal cells, shortly before the marked degeneration of CA1 pyramidal cells becomes visible. Extracellular field potentials in CA1 pyramidal layer revealed similar maximal population spike amplitudes of upon orthodromic stimu-

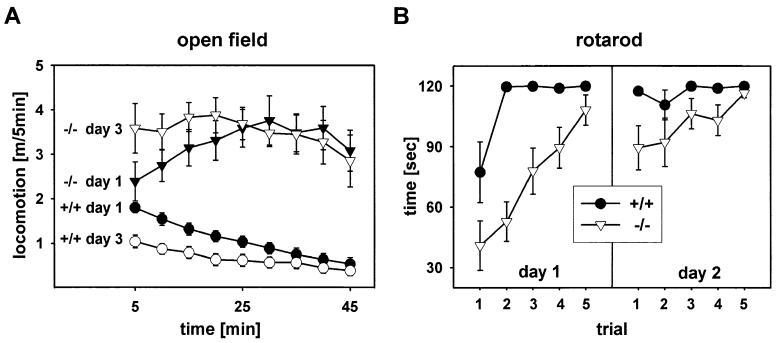

Figure 5. Behavioral Tests

(A) Locomotion of WT and KO mice in an open field test for 45 min (n = 12 each). The distance traveled over a period of 5 min is averaged for each time interval. WT mice adapted to the new environment by moving less, whereas the locomotion of KO mice increased.

(B) Rotarod test reveals inferior motor coordination of KO mice, which however improves with time. The time spent on the rotarod is shown. (n = 10 each). Error bars: SEM.

lation of the Schaffer collaterals (WT, 13.3 ± 2.5 mV; *Clcn3*$^{-/-}$, 10.7 ± 1.3 mV; $p > 0.4$, Mann-Whitney U test). Likewise, antidromic (axonal) stimulation in the alveus indicated similar excitability of CA1 pyramidal cells (maximal population spike amplitude 10.7 ± 2.3 mV [WT] versus 9.3 ± 1.7 mV [*Clcn3*$^{-/-}$]; $p > 0.7$). In order to reveal possible differences in excitatory synaptic transmission during sustained high-frequency activation, we generated a series of excitatory postsynaptic potentials (field-EPSPs) by repetitive (×50) high-frequency (50 Hz) stimulation of the Schaffer collateral. Fatigue of synaptic transmission was similar in WT and *Clcn3*$^{-/-}$ mice yielding 31% ± 3% and 34% ± 7% of the initial EPSP amplitude after 50 stimuli, respectively (5 slices from each group). Lastly, we probed the reaction of field responses to paired pulse stimulation, a test for local inhibitory circuitry and short-term plasticity (Figure 9A). Paired-pulse inhibition after 5 ms was similar in both groups, but paired-pulse potentiation at stimulus intervals between 10 and 200 ms was larger in WT mice. Thus, the only detected difference between WT and *Clcn3*$^{-/-}$ mice at the network level was a subtle change in short-term plasticity, without signs of impaired excitability or excitation–inhibition balance.

We then analyzed synaptic function at the microscopic level by recording pharmacologically isolated miniature excitatory and inhibitory currents (mEPSCs, Figure 9B, and mIPSCs, Figure 9D) from CA1 pyramidal cells. These currents represent the postsynaptic response to the presynaptic release of neurotransmitters that results from the fusion of single synaptic vesicles. The amplitude and frequency of mIPSCs was similar in both groups (Figure 9E). Glutamatergic mEPSCs were recorded in the presence of 200 mM sucrose in order to compensate for the low frequency of spontaneous events. While the difference in mean EPSC amplitude did not reach statistical significance possibly due the skewed distribution of EPSCs, the cumulative amplitude distributions were significantly shifted toward larger events in *Clcn3*$^{-/-}$ mice as compared to control (Figure 9C). Thus, elementary synaptic events are not reduced in *Clcn3*$^{-/-}$ mice, and glutamatergic EPSCs may even be slightly enlarged.

Discussion

Although a role of Cl^- channels in synaptic vesicle acidification and neurotransmitter uptake is well established, the molecular identity of these channels has remained elusive. We have now shown that ClC-3 is an intracellular chloride channel that copurifies with endosomal markers and is expressed in various types of synaptic vesicles. Surprisingly, the disruption of its gene in mice leads to a severe degeneration of the hippocampus and of photoreceptors. Before onset of major neuronal loss, network and synaptic functions in the hippocampus remain remarkably normal.

Roles of Intracellular Chloride Channels

Biophysical studies have revealed Cl^- conductances in many intracellular organelles (al-Awqati, 1995; Szewczyk, 1998), including the ER, Golgi, vesicles of the exo- and endocytotic pathways, lysosomes, and synaptic vesicles. Probably their main role consists in providing

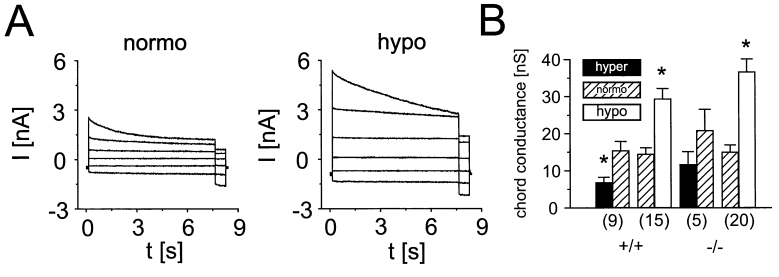

Figure 6. Swelling-Activated Chloride Currents

(A) Swelling-activated Cl^- currents from isolated hepatocytes recorded under symmetrical Cl^- in the whole-cell patch-clamp mode. Osmolarity was reduced from 300 mOsm (left, normo) to 200 mOsm (hypo). From −30 mV cells were clamped for 7 s to voltages between −80 and +120 mV. The recording is from a KO mouse, but currents were not different in WT. Chord conductance reversibly increased from 25.1 ± 3.7 to 44.0 ± 4.7 nS (n = 15) in WT and from 31.2 ± 3.1 to 47.8 ± 2.8 nS (n = 16) in KO.

(B) Swelling-sensitive Cl^- currents of pancreatic acinar cells. From nominally normotonic conditions, currents were increased by hypo- and decreased by hypertonicity. Currents were similar to those of hepatocytes (A). Mean chord conductance between −30 and +80 mV is shown. The number of measurements is given in brackets. Asterisks indicate significance at the $p < 0.05$ level. There was no significant difference between KO and WT.

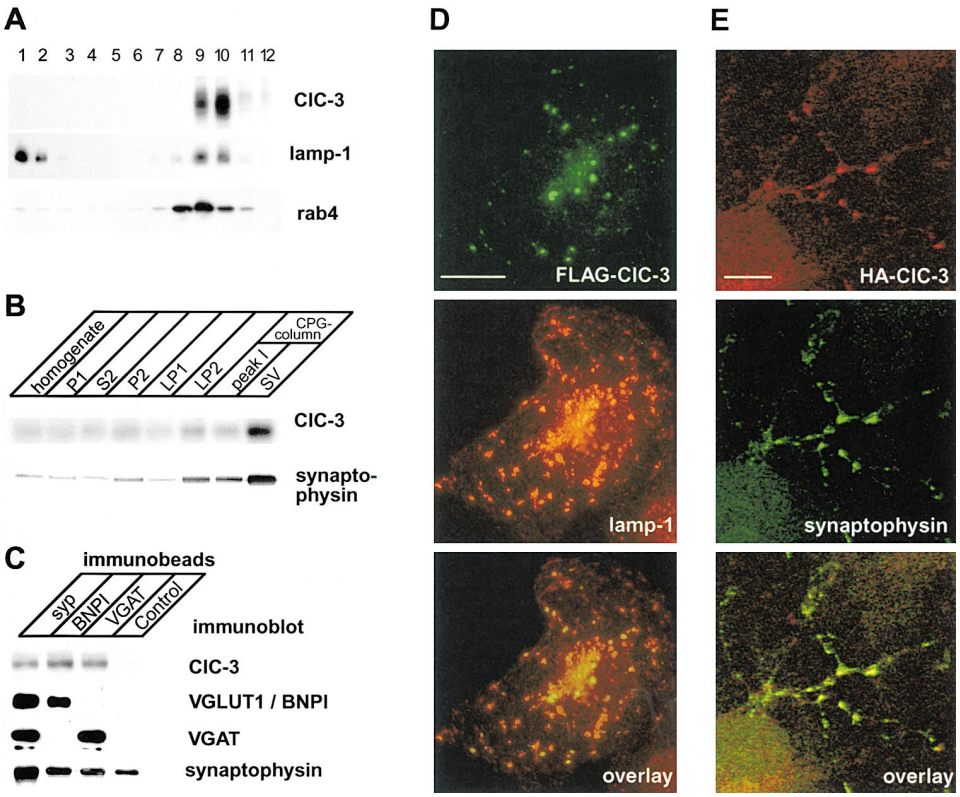

Figure 7. Subcellular Localization of ClC-3

(A) Western blots of Percoll gradient fractions isolated from mouse liver. ClC-3 and lamp-1 overlap in endosomal fractions (lanes 9 and 10). rab4 is exclusively found in endosomal fractions (lanes 8–11), while lamp-1 is additionally detected in lysosomal fractions (lanes 1 and 2).

(B) ClC-3 copurifies with synaptophysin. Synaptic vesicles were purified using established procedures, with the following fractions being analyzed: homogenate; P1, crude nuclear pellet; P2, crude synaptosomes (10,000 g pellet); S2, 10,000 g supernatant; LP1, 25,000 g pellet obtained after synaptosomal lysis; LP2, crude synaptic vesicles; Peak 1 and SV, large membrane and purified synaptic vesicles as separated by controlled pore glass (CPG) bead chromatography, respectively (see Huttner et al., 1983).

(C) ClC-3 is present on GABAergic and glutamatergic vesicles. Synaptic vesicles were isolated by microbeads coated with antibodies against synaptophysin, VGAT, and VGLUT1/BNPI. Immunoisolates were analyzed by Western blot.

(D) Immunofluorescence of transfected COS-7 cells. FLAG-ClC-3 is located on vesicular structures that overlapped with lamp-1.

(E) In cultured hippocampal neurons infected with recombinant Semliki Forest virus, HA-ClC-3 is located in punctate structures that were also stained for synaptophysin (scale bars: 10 μm).

an electrical shunt for the proton pump that acidifies their lumina. Proton pumping involves the transfer of both acid equivalents and electric charge. In contrast to acid equivalents, which are buffered rather efficiently, the charge is "buffered" only by the membrane capacitance. As a consequence, changes in pH are limited by the voltage generated across the vesicle membrane. The dissipation of this voltage by an electrical shunt allows for higher rates of proton transport. In many intracellular organelles, including endocytotic or synaptic vesicles, this shunt is provided by a Cl^- conductance, as also shown in the experiments of Figure 8B. Acidification of intracellular organelles serves various purposes: first, it is required for certain enzymatic activities that are, e.g., involved in lysosomal degradation or in the processing of prohormones. Second, the luminal pH is often crucial for receptor–ligand interactions, e.g., leading to a differential sorting of receptors and ligands (Dautry-Varsat et al., 1983). Luminal acidification is important for endocytosis and other vesicle trafficking (Mellman et al., 1986; Chapman and Munro, 1994). Finally, the electrochemical proton gradient provides the driving force for the transport of other substances across the vesicle membrane as in the concentrative uptake of neurotransmitters into synaptic vesicles (Reimer et al., 1998; Gasnier, 2000).

An intracellular role has been established for two other CLC channels. ClC-5 is crucial for the endocytotic uptake of proteins in the renal proximal tubule (Piwon et al., 2000). It is present in the early endocytotic pathway and colocalizes with the proton pump (Günther et al., 1998). The single CLC protein from *S. cerevisiae*, GEF1p, is located in a late Golgi compartment (Gaxiola et al., 1998; Schwappach et al., 1998). A disruption of either *GEF1* or *GEF2* (which encodes a subunit of the yeast V-type H^+-ATPase) leads to an iron-suppressible *petit* phenotype (Greene et al., 1993), linking again acidification to a CLC channel. Indeed, yeast strains disrupted for the CLC gene do not grow well at neutral or alkaline pH (Gaxiola et al., 1998; Schwappach et al., 1998). Disrupting *GEF1* also affects the quality control of membrane proteins (Li et al., 1999). There may also be a direct effect of intravesicular Cl^- on enzymatic activity (Davis-Kaplan et al., 1998), suggesting a role of vesicular

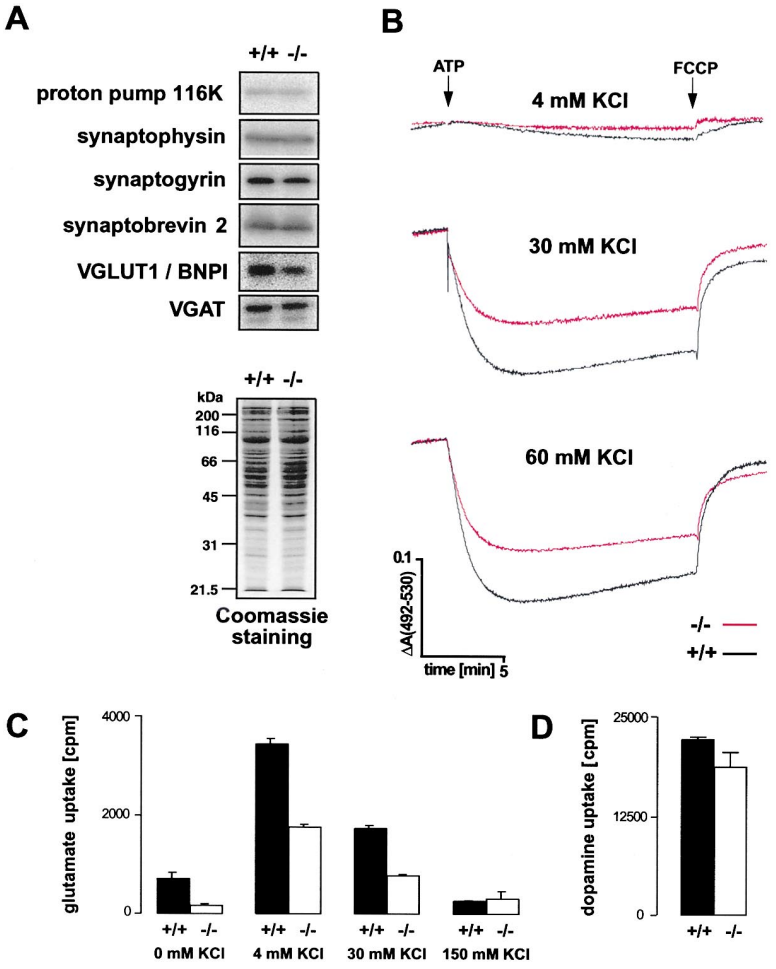

Figure 8. Characterization of Synaptic Vesicles

(A) Western blot of LP2 preparations from WT and KO mice probed for several synaptic markers. Below is a Coomassie staining of an SDS–PAGE.

(B) ATP-induced acidification in LP2 fractions of WT and KO mice at different Cl^- concentrations measured by acridine orange absorbance (downward deflection represents acidification).

(C) Chloride dependence of glutamate uptake in LP2 fractions of WT and KO mice.

(D) Dopamine uptake in LP2 fractions of WT and KO mice.

Cl^- channels that is independent of the formation of electrical shunts.

ClC-3 Is an Endosomal Cl^- Channel that Has a Role in Synaptic Vesicle Acidification

Our cell fractionation and immunofluorescence of transfected cells suggests that ClC-3 resides in an endosomal compartment. Additionally, ClC-3 is clearly expressed on synaptic vesicles. These localizations are mutually consistent, as synaptic vesicles are recycled by endocytosis at the synaptic terminal (Südhof, 1995). Moreover, many synaptic vesicle proteins are targeted to endosomes when expressed in nonneuronal cells (Linstedt and Kelly, 1991; Liu and Edwards, 1997).

ClC-3 has a role in intravesicular acidification, as we have shown here for synaptic vesicles. The electrochemical proton gradient across synaptic vesicle membranes drives the uptake of neurotransmitters. The transport of monoamines and acetylcholine depends predominantly on ΔpH, whereas the electrical component $\Delta\Psi$ of this gradient is more important for the uptake of GABA and even more so for glutamate (Reimer et al., 1998; Bellocchio et al., 2000). A vesicular Cl^- conductance will increase ΔpH at the expense of $\Delta\Psi$. Conversely, downregulating Cl^- channels will decrease ΔpH and increase $\Delta\Psi$. This will enhance the uptake of glutamate, as its vesicular transporter is primarily driven by $\Delta\Psi$ (Maycox et al., 1988; Bellocchio et al., 2000), but will reduce the vesicular enrichment of monoamines and acetylcholine. However, we found no change in the chloride dependence of steady-state glutamate uptake, although changes affecting only a subpopulation of glutamatergic vesicles may not have been resolved. The effect on GABA uptake is difficult to predict, as the dependence of its transporter on both ΔpH and $\Delta\Psi$ may result in little change. Indeed, miniature inhibitory postsynaptic currents (mIPSCs), which represent postsynaptic currents elicited by the presynaptic exocytosis of single GABAergic vesicles, were not significantly changed in hippocampal neurons from *Clcn3*$^{-/-}$ mice. In contrast, there was a slight shift toward larger amplitudes of miniature excitatory postsynaptic currents (mEPSCs), consistent with a predicted increase of $\Delta\Psi$ in synaptic vesicles of KO mice that should in turn raise their glutamate content. In apparent contrast to these electrophysiological findings from juvenile tissue, the uptake of glutamate into synaptic vesicles isolated from whole brains of adult *Clcn3*$^{-/-}$ mice was decreased. However, at this stage the amount of the vesicular glutamate transporter VGLUT1/BNPI was also reduced (Figure 8A), compatible with a selective loss of glutamatergic vesicles or neurons in KO mice. Thus, it remains possible that at physiological chloride

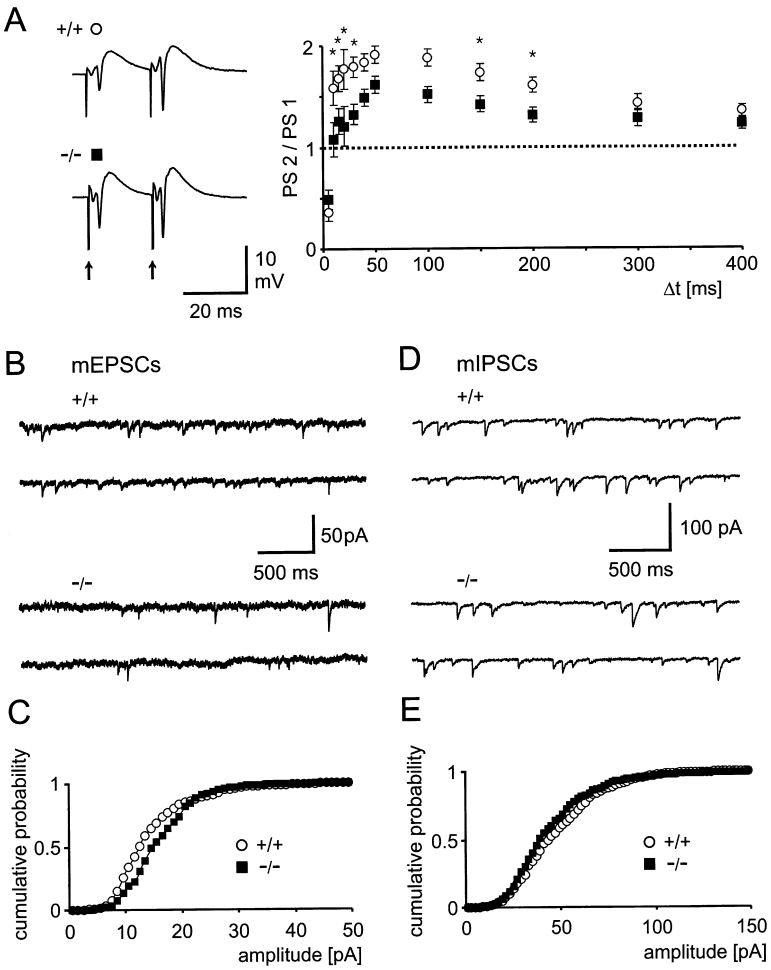

Figure 9. Electrophysiology of CA1 Neurons

(A) Field response in CA1 pyramidal layer to paired-pulse stimulation (indicated by arrows) of Schaffer collaterals. Stimulation intensity was adjusted to 70% of the maximal evoked response in each slice. This was not different between WT (13.3 ± 2.5 mV, mean ± SEM, n = 8) and KO mice (10.7 ± 1.3 mV, n = 14; not different at $p > 0.4$, Mann-Whitney U test). WT mice display stronger paired-pulse facilitation of the second response at most intervals between 10–200 ms (asterisks, $p < 0.05$). Sample responses (left panels) shown for $\Delta t = 20$ ms.

(B) Miniature excitatory currents (mEPSCs) recorded in CA1 pyramidal cells.

(C) Cumulative amplitude histogram of mEPSCs pooled from 8 WT and 7 KO cells, respectively. The amplitude distribution is shifted to the right, indicating larger mEPSCs in KO mice ($p < 0.001$, Kolmogorov-Smirnov test). Mean mEPSC amplitudes were not different (WT: 14.8 ± 1.3 pA, n = 8; KO: 16.5 ± 1.0 pA, n = 7; $p > 0.3$).

(D) Miniature inhibitory currents (mIPSCs). No obvious difference in amplitude or frequency is apparent. Amplitude calibration differs from (B).

(E) Cumulative amplitude histogram of mIPSCs pooled from 5 WT and 4 KO cells, respectively. No difference in the distribution of amplitudes ($p = 0.5$, K-S test) or in mean amplitudes ($p > 0.4$, Wilcoxon) was found. Likewise, the frequency or interevent–interval distribution of mIPSCs did not differ.

concentrations the glutamate content of the remaining glutamatergic vesicles is increased. Our macroscopic field potential recordings in slices from juvenile hippocampi suggest that as long as glutamatergic principal cells exist in *Clcn3*$^{-/-}$ mice, their excitability, synaptic efficacy, and fatigue are largely normal. The slight loss in short-term plasticity indicated by the decreased paired-pulse potentiation may indicate the beginning malfunction of hippocampal neurons toward the end of the second postnatal week but does not explain the subsequent neuronal loss.

The disruption of a synaptic vesicle Cl^- channel should have differential effects on the uptake of neurotransmitters, whereas an inhibition of the H^+-ATPase should impair the accumulation of all classical neurotransmitters. As a consequence, both mIPSCs and mEPSCs were decreased when the H^+-ATPase was specifically inhibited by bafilomycin (Zhou et al., 2000).

ClC-3 Disruption Causes a Severe but Selective Neurodegeneration

The finding that the acidification of synaptic vesicles from KO mice was reduced but still dependent on Cl^-, the only subtle changes in postsynaptic miniature currents, and the selective neurodegeneration suggest that ClC-3 is not the only neuronal vesicular Cl^- channel. Different expression patterns of ClC-3 and of other Cl^- channels might be invoked to explain the region-specific degeneration of *Clcn3*$^{-/-}$ mice. However, among the closely related ClC-4 and ClC-5 Cl^- channels, ClC-5 is only weakly expressed in brain (Steinmeyer et al., 1995) and ClC-4 is abundantly expressed in the hippocampus and the cerebellum (Adler et al., 1997). As this distribution is similar to that of ClC-3, it cannot explain the differential degeneration of the hippocampus. Further, there was no upregulation of either ClC-4 or ClC-5 in brains of *Clcn3*$^{-/-}$ mice (Figure 3). On the other hand, the selective degeneration observed in *Clcn3*$^{-/-}$ mice may be due to the known high vulnerability of both the hippocampus and photoreceptors. In fact, the CA1 region, the brain area that degenerates first in KO mice, is among the first CNS structures to show cell death after anoxia, glutamate toxicity, or epileptic seizures (Nunn et al., 1994; Grooms et al., 2000).

It is tempting to speculate that the neuronal degeneration in *Clcn3*$^{-/-}$ mice is caused by glutamate toxicity that is due to a higher glutamate content of synaptic vesicles. This might apply for hippocampal neurons but probably not for photoreceptors because these cells are quite insensitive to activators of glutamate receptors (Facci et al., 1990). On the other hand, ClC-3 is not present exclusively on synaptic vesicles, but is ex-

pressed in many nonneuronal tissues, where it colocalizes with markers for (late) endosomal compartments. In addition to its role in synaptic vesicles, ClC-3 may function in endosomal compartments of neurons as well. A defective acidification in the endosomal or recycling pathway may lead to a mislocalization of membrane proteins (including transporters and receptors), to altered luminal receptor–ligand interactions, or to changes in luminal enzymatic activities. Any of these events could contribute to the severe neurodegeneration in *Clcn3*$^{-/-}$ mice.

It seems surprising that mice almost totally lacking the hippocampus can survive for more than a year. However, humans whose hippocampi were almost totally removed by surgery in early attempts to cure severe epilepsy survived and mainly showed selective memory deficits (Scoville and Millner, 1957). The hippocampus is thought to be important for spatial learning, but the blindness of *Clcn3*$^{-/-}$ mice makes classical learning tests difficult to interpret. The ability of KO mice to learn motor skills shows that other forms of plasticity that are largely independent of the hippocampus are preserved in these animals. Rats whose hippocampi were destroyed show increased locomotion and hyperactivity (Coutureau et al., 2000), suggesting that this aspect of our model may be entirely explained by the degeneration of the hippocampus.

In summary, our work has revealed that ClC-3 is an intracellular chloride channel. It is also present on synaptic vesicles, where it contributes to their acidification. The phenotype of the present knockout mice strongly suggests that ClC-3 is not the only Cl^- channel of synaptic vesicles, and we expect that other CLC channels may have similar roles. Our work provides a basis for investigating a possible regulation of neurotransmitter accumulation by modulating vesicular Cl^- channels, which is known from neuroendocrine cells (Tamir et al., 1994). Although it is presently unclear whether the neurodegeneration in *Clcn3*$^{-/-}$ mice is directly related to its role in synaptic vesicles, the importance of the ClC-3 Cl^- channel for the central nervous system is underscored by the severe phenotype resulting from its disruption.

Experimental Procedures

Disruption of the *Clcn3* Gene

A ~19 kb clone containing the first 6 exons and promoter region of *Clcn3* was isolated from a 129/SvJ mouse genomic library in λFixII (Stratagene). A 2.6 kb KpnI–ApaI fragment from exon and intron 2 and a NcoI fragment from intron 3 to intron 5 were placed in pKO Scrambler V901 vector (Lexicon Genetics), flanking a phosphoglycerate kinase (pgk) promoter-driven neomycin resistance cassette. This deletes a 1 kb fragment of *Clcn3* that contains exon 3. Splicing from exon 2 to exon 4 would result in a frameshift. A pgk promoter-driven diphteria toxin A cassette was added. The construct was electroporated into R1 ES cells. Clones resistant to G418 were analyzed and cells from two correctly targeted clones were injected into C57BL/6 blastocysts. Resulting male chimeras were bred with C57BL/6 females. Heterozygous animals stemming from two different ES cell clones were inbred to yield *Clcn3*$^{-/-}$ homozygous mutants. All experiments were performed on littermates with C57BL/6-129SV mixed background.

Generation and Characterization of ClC-3 Antibodies

Antisera were raised in rabbits against a peptide (CKDRERHRRIN SKKKE-amide) that represents a part of the ClC-3 amino terminus. Two antisera (3A4 and 3A6) proved useful in Western blots (at 1:1000 and 1:500 dilution, respectively). They were affinity-purified and tested for cross-reactivity against ClC-4 and ClC-5 as in Günther et al. (1998). Their specificity was verified by comparing Western blots of WT and *Clcn3*$^{-/-}$ mice. They were less sensitive in immunocytochemistry, making it impossible to investigate ClC-3 localization in brain by immunohistochemistry. A commercial ClC-3 antibody (Alomone/Chemicon) is unsuited for immunofluorescence and detects a band that is not abolished in *Clcn3*$^{-/-}$ mice.

Light and Electron Microscopy and In Situ Hybridization

To analyze brain tissue, mice were perfused transcardially with 4% paraformaldehyde (PFA) in PBS for 5 min. For Nissl staining, brains were fixed overnight in 4% PFA at 4°C, paraffin embedded, and 5 μm sections cut. For Griffonia Simplicifolia Agglutinin (GSA) histochemistry, 7 μm sections were incubated with biotinylated GSA (Vector) (1:50) and then labeled using the Avidin-Biotin Elite system (Vector). Retinal immunostaining was as described (Haverkamp and Wässle, 2000). To detect VGLUT1/BNPI, eyes were fixed in 4% PFA. For the 3A6 antibody we used 4% EDAC (Sigma). Antibody dilutions were 1:100 (3A6) and 1:2500 (BNPI). Sections were examined by confocal microscopy (Leica TCS). For high-power micrographs and electron microscopy, mice were perfused with 4% PFA and 1% glutaraldehyde in PBS. Tissues were postfixed in 1% OsO_4, dehydrated, and embedded in Epon. Sections (0.5 μm) were stained with methylene blue. Ultrathin sections (60 nm) were stained with uranylacetate and lead citrate and examined with a Zeiss EM 902. In situ hybridization with ClC-3-specific N-terminal 510 nt cRNA probes was done essentially as in Hartmann et al. (1995).

Expression and Detection of ClC-3 in COS Cells and in Rat Hippocampal Neurons

Human ClC-3 containing a FLAG epitope at E178 was cloned into pCIneo (Promega). Transfection and immunofluorescence of COS-7 cells was as described (Günther et al., 1998). The lamp-1 antibody was from Dr. Carlsson. Expression in neurons used the Semliki Forest Virus system (Owe-Larsson et al., 1999). ClC-3 containing an HA epitope after E178 was cloned into pSFV1 (Life Technologies). Cultures of rat hippocampal neurons (Neuhoff et al., 1999) were incubated after 7–14 days with activated recombinant virus. After 1.5 hr, the medium was exchanged and cells were cultured for 6–7 hr. Cells were fixed, blocked, and permeabilized, and incubated with antibodies (anti-HA (3F10), Roche; anti-synaptophysin, Synaptic Systems, Germany). After washing, they were incubated with secondary antibodies (Molecular Probes), washed, embedded, and analyzed by confocal microscopy (Leica TCS).

Cell Fractionation of Liver Membranes

Livers were minced and homogenized in 10 vol of 250 mM sucrose and 3 mM imidazol (pH 7.4) using a Potter-Elvehjem (5 strokes, 500 rpm). The homogenate was centrifuged twice (10 min at 1000 × g and 10 min at 3000 × g). The supernatant was fractionated on a Percoll gradient (Braun et al., 1989). Western analysis of fractions used antibodies against ClC-3 (3A4), rab4 (Santa Cruz), and lamp-1. The latter antibody (1D4B) developed by J. T. August (Baltimore) was obtained from the Developmental Studies Hybridoma Bank (Iowa).

Purification of Synaptic Vesicles, Acidification Assays, and Uptake of Neurotransmitters

Synaptic vesicles were purified as described (Huttner et al., 1983; Takamori et al., 2000b). Synaptic vesicles were immunoisolated using antibodies directed against synaptic vesicle proteins as described (Takamori et al., 2000b). Luminal acidification was measured using acridine orange as described (Hartinger and Jahn, 1993). Uptake of ^{3}H-labeled neurotransmitters into synaptic vesicles was measured as described (Hell et al., 1988) with a slight modification. LP2 fractions from wild-type and KO mice were resuspended in assay buffer (290 mM sucrose, 30 mM KCl, 4 mM $MgSO_4$, and 10 mM HEPES-KOH [pH 7.4]), and 25 μg LP2/reaction were used for one measurement. FCCP-sensitive uptake activities were determined by subtracting the nonspecific accumulation of neurotransmitters in presence of 46 μM FCCP.

Measurements of Swelling-Activated Chloride Currents

Pancreatic acini were prepared (Zdebik et al., 1997) and clusters of 5–10 cells were held by a suction pipette. Hepatocyte preparation was adapted from Dittmer et al. (1999). Low Ca^{2+} Ringer solution was perfused through the portal vein for 20 min. Livers were dissected, minced, and cells were dissociated by pipetting. Single hepatocytes on glass coverslips were patched after 1–2 days in RPMI 1640/10% FCS. Extracellular solution for patch-clamping pancreatic cells contained (in mM): NMDG 70, HEPES 3 (pH 7.4), $MgCl_2$ 1, glucose 5, $BaCl_2$ 5, TEA-Cl 5, and 0, 160, and 240 mM mannitol to obtain hypo-, iso-, and hypertonic solutions. 1-octanol (0.5 mM) was added to block gap junctions. For hepatocytes, extracellular saline was NaCl 95, KH_2PO_4 0.4, K_2HPO_4 1.6, glucose 5, $MgCl_2$ 1, Ca-gluconate 1.3 (pH 7.4). Osmolarity was adjusted by adding 100 or 200 mM mannitol. The pipette contained (in mM): NMDG 150, EGTA 5, HEPES 5, MgATP 3, Ca-gluconate 1.9, glucose 5 (pH 7.2). Free Ca^{2+} was 10^{-7} M. In some experiments, NMDG-Cl was replaced by CsCl. Access resistance was below 5 MΩ. Experiments were performed at 37°C. Chord conductances were determined 2 min after solution change.

Hippocampal Slice Electrophysiology

Horizontal hippocampal slices (400 μm) were prepared from juvenile mice (P13-P15) using standard methods. Field potential recordings were performed in an interface chamber at 35°C, patch-clamp experiments under submerged conditions at 26°C–29°C. Extracellular solution was artificial cerebrospinal fluid (ACSF) containing (in mM): NaCl 129, $NaHCO_3$ 21, KCl 3, NaH_2PO_4 1.25, $CaCl_2$ 1.6, $MgSO_4$ 1.8, glucose 10, saturated with 95% O_2/5% CO_2 (pH 7.4). Field potentials were recorded with ~4 MΩ glass microelectrodes, low-pass filtered at 3 kHz, and sampled at 8 kHz (Signal Averager software, CED). For presynaptic stimulation, we used bipolar platinum electrodes (100 μs square pulses). Patch pipettes (2–5 MΩ) were filled with (in mM): CsCl 125, $MgCl_2$ 2, $CaCl_2$ 2, HEPES 10, EGTA 10 (pH 7.3). Cells were held at −60 mV and miniature IPSCs were isolated by bath application of 10 μM NBQX, 30 μM APV, and 0.5 μM TTX. Miniature EPSCs were isolated by 20 μM bicuculline and 0.5 μM TTX. The low frequency of spontaneous mEPSCs (~1/min) was increased by adding 200 mM sucrose to the bath. Recordings were only used as long as regularly applied voltage pulses revealed stable series resistance. Data were stored on video tape and analyzed offline with the SCAN and CDR software written by Dr. J. Dempster, University of Strathclyde, UK.

Electroretinograms

Electroretinograms (ERGs) were recorded in 15 KO, 6 heterozygous, and 2 WT animals. Mice were anesthetized by 20 mg xylazin and 40 mg ketamine per kg. Pupils were dilated with 1% atropine and 0.5% tropicamide. ERGs were recorded using a monopolar electrode with a plastic-embedded wire loop (ϕ; 3 mm) and two subcutaneous silver needles as reference (3 mm below the eye) and ground electrode (forehead). Mice were dark adapted for 2 hr and were then placed in a Ganzfeld bowl (Multiliner Vision, Toennies). Flash energies ranged from 4×10^{-4} to 3 cds/m^2. Details of the method have been published (Ruether et al., 1997).

Behavioral Tests

Basal activity was measured using a actimot system (TSE, Germany). Single-caged animals were observed over at least 72 hr and overall activity and resting times were calculated for an average 24 hr period. Open field tests were performed in chambers (50 × 50 × 50 cm) monitored by an automated video system (TSE). Mice were placed in the chambers for 45 min on 3 consecutive days. The traveled distance was analyzed in 5 min steps. The illumination in the central zone was 150 lux. The rotarod test system (TSE) consisted of five gritted plastic rollers each flanked by round plates to separate chambers. It was driven with 5 rpm. The time each mouse remained on the roller was measured (up to 120 s). Five trials per mouse on 2 consecutive days were performed.

Acknowledgments

We thank B. Merz for technical assistance, D. Kasper for help with cell fractionation, I. Hermans-Borgmeyer and S. Fehr for help with in situ hybridization and RNAse protection assays, C. Hübner for helping to prepare hepatocytes, V. Stein and N. Maier for initial electrophysiological experiments, and S. Carlsson for the antibody against lamp-1. Supported by grants from the DFG, the Gottfried Wilhelm Leibniz prize, and the Louis-Jeantet prize for medicine to T. J. J., by the Gottfried Wilhelm Leibniz prize to R. J., and the DFG to K. R.

Received September 20, 2000; revised December 6, 2000.

References

Adler, D.A., Rugarli, E.I., Lingenfelter, P.A., Tsuchiya, K., Poslinski, D., Liggitt, H.D., Chapman, V.M., Elliott, R.W., Ballabio, A., and Disteche, C.M. (1997). Evidence of evolutionary up-regulation of the single active X chromosome in mammals based on *Clc4* expression levels in Mus spretus and Mus musculus. Proc. Natl. Acad. Sci. USA *94*, 9244–9248.

al-Awqati, Q. (1995). Chloride channels of intracellular organelles. Curr. Opin. Cell Biol. *7*, 504–508.

Bellocchio, E.E., Hu, H., Pohorille, A., Chan, J., Pickel, V.M., and Edwards, R.H. (1998). The localization of the brain-specific inorganic phosphate transporter suggests a specific presynaptic role in glutamatergic transmission. J. Neurosci. *18*, 8648–8659.

Bellocchio, E.E., Reimer, R.J., Fremeau, R.T., Jr., and Edwards, R.H. (2000). Uptake of glutamate into synaptic vesicles by an inorganic phosphate transporter. Science *289*, 957–960.

Borsani, G., Rugarli, E.I., Taglialatela, M., Wong, C., and Ballabio, A. (1995). Characterization of a human and murine gene (*CLCN3*) sharing similarities to voltage-gated chloride channels and to a yeast integral membrane protein. Genomics *27*, 131–141.

Braun, M., Waheed, A., and von Figura, K. (1989). Lysosomal acid phosphatase is transported to lysosomes via the cell surface. EMBO J. *8*, 3633–3640.

Chapman, R.E., and Munro, S. (1994). Retrieval of TGN proteins from the cell surface requires endosomal acidification. EMBO J. *13*, 2305–2312.

Coutureau, E., Galani, R., Jarrard, L.E., and Cassel, J.C. (2000). Selective lesions of the entorhinal cortex, the hippocampus, or the fimbria-fornix in rats: a comparison of effects on spontaneous and amphetamine-induced locomotion. Exp. Brain Res. *131*, 381–392.

Dautry-Varsat, A., Ciechanover, A., and Lodish, H.F. (1983). pH and the recycling of transferrin during receptor-mediated endocytosis. Proc. Natl. Acad. Sci. USA *80*, 2258–2262.

Davis-Kaplan, S.R., Askwith, C.C., Bengtzen, A.C., Radisky, D., and Kaplan, J. (1998). Chloride is an allosteric effector of copper assembly for the yeast multicopper oxidase Fet3p: an unexpected role for intracellular chloride channels. Proc. Natl. Acad. Sci. USA *95*, 13641–13645.

Dittmer, F., Ulbrich, E.J., Hafner, A., Schmahl, W., Meister, T., Pohlmann, R., and von Figura, K. (1999). Alternative mechanisms for trafficking of lysosomal enzymes in mannose 6-phosphate receptor-deficient mice are cell type-specific. J. Cell Sci. *112*, 1591–1597.

Duan, D., Winter, C., Cowley, S., Hume, J.R., and Horowitz, B. (1997). Molecular identification of a volume-regulated chloride channel. Nature *390*, 417–421.

Facci, L., Leon, A., and Skaper, S.D. (1990). Excitatory amino acid neurotoxicity in cultured retinal neurons: involvement of N-methyl-D-aspartate (NMDA) and non-NMDA receptors and effect of ganglioside GM1. J. Neurosci. Res. *27*, 202–210.

Friedrich, T., Breiderhoff, T., and Jentsch, T.J. (1999). Mutational analysis demonstrates that ClC-4 and ClC-5 directly mediate plasma membrane currents. J. Biol. Chem. *274*, 896–902.

Gasnier, B. (2000). The loading of neurotransmitters into synaptic vesicles. Biochimie *82*, 327–337.

Gaxiola, R.A., Yuan, D.S., Klausner, R.D., and Fink, G.R. (1998). The yeast CLC chloride channel functions in cation homeostasis. Proc. Natl. Acad. Sci. USA *95*, 4046–4050.

Greene, J.R., Brown, N.H., DiDomenico, B.J., Kaplan, J., and Eide, D.J. (1993). The GEF1 gene of Saccharomyces cerevisiae encodes

an integral membrane protein; mutations in which have effects on respiration and iron-limited growth. Mol. Gen. Genet. *241*, 542–553.

Grooms, S.Y., Opitz, T., Bennett, M.V., and Zukin, R.S. (2000). Status epilepticus decreases glutamate receptor 2 mRNA and protein expression in hippocampal pyramidal cells before neuronal death. Proc. Natl. Acad. Sci. USA *97*, 3631–3636.

Günther, W., Lüchow, A., Cluzeaud, F., Vandewalle, A., and Jentsch, T.J. (1998). ClC-5, the chloride channel mutated in Dent's disease, colocalizes with the proton pump in endocytotically active kidney cells. Proc. Natl. Acad. Sci. USA *95*, 8075–8080.

Hartinger, J., and Jahn, R. (1993). An anion binding site that regulates the glutamate transporter of synaptic vesicles. J. Biol. Chem. *268*, 23122–23127.

Hartmann, D., Fehr, S., Meyerhof, W., and Richter, D. (1995). Distribution of somatostatin receptor subtype 1 mRNA in the developing cerebral hemispheres of the rat. Dev. Neurosci. *17*, 246–255.

Haverkamp, S., and Wässle, H. (2000). Immunocytochemical analysis of the mouse retina. J. Comp. Neurol. *424*, 1–23.

Hell, J.W., Maycox, P.R., Stadler, H., and Jahn, R. (1988). Uptake of GABA by rat brain synaptic vesicles isolated by a new procedure. EMBO J. *7*, 3023–3029.

Huttner, W.B., Schiebler, W., Greengard, P., and De Camilli, P. (1983). Synapsin I (protein I), a nerve terminal-specific phosphoprotein. III. Its association with synaptic vesicles studied in a highly purified synaptic vesicle preparation. J. Cell Biol. *96*, 1374–1388.

Jentsch, T.J., Friedrich, T., Schriever, A., and Yamada, H. (1999). The CLC chloride channel family. Pflügers Arch. *437*, 783–795.

Kawasaki, M., Uchida, S., Monkawa, T., Miyawaki, A., Mikoshiba, K., Marumo, F., and Sasaki, S. (1994). Cloning and expression of a protein kinase C-regulated chloride channel abundantly expressed in rat brain neuronal cells. Neuron *12*, 597–604.

Kawasaki, M., Suzuki, M., Uchida, S., Sasaki, S., and Marumo, F. (1995). Stable and functional expression of the ClC-3 chloride channel in somatic cell lines. Neuron *14*, 1285–1291.

Li, Y., Kane, T., Tipper, C., Spatrick, P., and Jenness, D.D. (1999). Yeast mutants affecting possible quality control of plasma membrane proteins. Mol. Cell. Biol. *19*, 3588–3599.

Linstedt, A.D., and Kelly, R.B. (1991). Synaptophysin is sorted from endocytotic markers in neuroendocrine PC12 cells but not transfected fibroblasts. Neuron *7*, 309–317.

Liu, Y., and Edwards, R.H. (1997). Differential localization of vesicular acetylcholine and monoamine transporters in PC12 cells but not CHO cells. J. Cell Biol. *139*, 907–916.

Lloyd, S.E., Pearce, S.H., Fisher, S.E., Steinmeyer, K., Schwappach, B., Scheinman, S.J., Harding, B., Bolino, A., Devoto, M., Goodyer, P., et al. (1996). A common molecular basis for three inherited kidney stone diseases. Nature *379*, 445–449.

Matsumura, Y., Uchida, S., Kondo, Y., Miyazaki, H., Ko, S.B., Hayama, A., Morimoto, T., Liu, W., Arisawa, M., Sasaki, S., and Marumo, F. (1999). Overt nephrogenic diabetes insipidus in mice lacking the CLC-K1 chloride channel. Nat. Genet. *21*, 95–98.

Maycox, P.R., Deckwerth, T., Hell, J.W., and Jahn, R. (1988). Glutamate uptake by brain synaptic vesicles. Energy dependence of transport and functional reconstitution in proteoliposomes. J. Biol. Chem. *263*, 15423–15428.

McIntire, S.L., Reimer, R.J., Schuske, K., Edwards, R.H., and Jorgensen, E.M. (1997). Identification and characterization of the vesicular GABA transporter. Nature *389*, 870–876.

Mellman, I., Fuchs, R., and Helenius, A. (1986). Acidification of the endocytic and exocytic pathways. Annu. Rev. Biochem. *55*, 663–700.

Neuhoff, H., Roeper, J., and Schweizer, M. (1999). Activity-dependent formation of perforated synapses in cultured hippocampal neurons. Eur. J. Neurosci. *11*, 4241–4250.

Nunn, J.A., LePeillet, E., Netto, C.A., Hodges, H., Gray, J.A., and Meldrum, B.S. (1994). Global ischaemia: hippocampal pathology and spatial deficits in the water maze. Behav. Brain Res. *62*, 41–54.

Owe-Larsson, B., Berglund, M., Kristensson, K., Garoff, H., Larhammar, D., Brodin, L., and Low, P. (1999). Perturbation of the synaptic release machinery in hippocampal neurons by overexpression of SNAP-25 with the Semliki Forest virus vector. Eur. J. Neurosci. *11*, 1981–1987.

Piwon, N., Günther, W., Schwake, R., Bösl, M.R., and Jentsch, T.J. (2000). ClC-5 Cl^- channel disruption impairs endocytosis in a mouse model for Dent's disease. Nature *408*, 369–373.

Reimer, R.J., Fon, E.A., and Edwards, R.H. (1998). Vesicular neurotransmitter transport and the presynaptic regulation of quantal size. Curr. Opin. Neurobiol. *8*, 405–412.

Ruether, K., van de Pol, D., Jaissle, G., Berger, W., Tornow, R.P., and Zrenner, E. (1997). Retinoschisislike alterations in the mouse eye caused by gene targeting of the Norrie disease gene. Invest. Ophthalmol. Vis. Sci. *38*, 710–718.

Schwappach, B., Stobrawa, S., Hechenberger, M., Steinmeyer, K., and Jentsch, T.J. (1998). Golgi localization and functionally important domains in the NH_2 and COOH terminus of the yeast CLC putative chloride channel Gef1p. J. Biol. Chem. *273*, 15110–15118.

Scoville, W., and Millner, B. (1957). Loss of recent memory after bilateral hippocampal lesions. J. Neurol. Neurosurg. Psychiatry *20*, 11–21.

Shimada, K., Li, X., Xu, G., Nowak, D.E., Showalter, L.A., and Weinman, S.A. (2000). Expression and canalicular localization of two isoforms of the ClC-3 chloride channel from rat hepatocytes. Am. J. Physiol. *279*, G268–G276.

Simon, D.B., Bindra, R.S., Mansfield, T.A., Nelson-Williams, C., Mendonca, E., Stone, R., Schurman, S., Nayir, A., Alpay, H., Bakkaloglu, A., et al. (1997). Mutations in the chloride channel gene, CLCNKB, cause Bartter's syndrome type III. Nat. Genet. *17*, 171–178.

Steinmeyer, K., Klocke, R., Ortland, C., Gronemeier, M., Jockusch, H., Gründer, S., and Jentsch, T.J. (1991). Inactivation of muscle chloride channel by transposon insertion in myotonic mice. Nature *354*, 304–308.

Steinmeyer, K., Schwappach, B., Bens, M., Vandewalle, A., and Jentsch, T.J. (1995). Cloning and functional expression of rat CLC-5, a chloride channel related to kidney disease. J. Biol. Chem. *270*, 31172–31177.

Südhof, T.C. (1995). The synaptic vesicle cycle: a cascade of protein-protein interactions. Nature *375*, 645–653.

Szewczyk, A. (1998). The intracellular potassium and chloride channels: properties, pharmacology and function. Mol. Membr. Biol. *15*, 49–58.

Takamori, S., Rhee, J.S., Rosenmund, C., and Jahn, R. (2000a). Identification of a vesicular glutamate transporter that defines a glutamatergic phenotype in neurons. Nature *407*, 189–194.

Takamori, S., Riedel, D., and Jahn, R. (2000b). Immunoisolation of GABA-specific synaptic vesicles defines a functionally distinct subset of synaptic vesicles. J. Neurosci. *20*, 4904–4911.

Tamir, H., Piscopo, I., Liu, K.P., Hsiung, S.C., Adlersberg, M., Nicolaides, M., al-Awqati, Q., Nunez, E.A., and Gershon, M.D. (1994). Secretogogue-induced gating of chloride channels in the secretory vesicles of parafollicular cells. Endocrinology *135*, 2045–2057.

Zdebik, A., Hug, M.J., and Greger, R. (1997). Chloride channels in the luminal membrane of rat pancreatic acini. Pflügers Arch. *434*, 188–194.

Zhou, Q., Petersen, C.C., and Nicoll, R.A. (2000). Effects of reduced vesicular filling on synaptic transmission in rat hippocampal neurones. J. Physiol. Lond. *525*, 195–206.

Note Added in Proof

Parallel to this work it has been shown that the ClC-7 chloride channel resides in late endosomal to lysosomal compartments and is involved in the acidification of the resorption lacuna formed by osteoclasts. Its disruption leads to osteopetrosis: Kornak, U., Kasper, D., Bösel, M.R., Kaiser, E., Schweizer, M., Schulz, A., Friedrich, W., Delling, G., and Jentsch, T.J. (2001). Loss of the ClC-7 chloride channel leads to osteopetrosis in mice and man. Cell *104* (January 26 issue), in press.